Journal of Computational Physics 376 (2019) 1089–1107

Contents lists available at ScienceDirect

Journal of Computational Physics

www.elsevier.com/locate/jcp

Boundary conditions for two-sided fractional diffusion

James F. Kelly *, Harish Sankaranarayanan, Mark M. Meerschaert

Department of Statistics and Probability, Michigan State University, East Lansing, MI 48824, USA

ARTICLE INFO

Article history:
Received 14 March 2018
Received in revised form 29 September 2018
Accepted 4 October 2018
Available online 5 October 2018

Keywords:
Fractional calculus
Boundary conditions
Riesz derivative
Stability analysis

ABSTRACT

This paper develops appropriate boundary conditions for the two-sided fractional diffusion equation, where the usual second derivative in space is replaced by a weighted average of positive (left) and negative (right) fractional derivatives. Mass preserving, reflecting boundary conditions for two-sided fractional diffusion involve a balance of left and right fractional derivatives at the boundary. Stable, consistent explicit and implicit Euler methods are detailed, and steady state solutions are derived. Steady state solutions for two-sided fractional diffusion equations using both Riemann–Liouville and Caputo flux are computed. For Riemann–Liouville flux and reflecting boundary conditions, the steady-state solution is singular at one or both of the end-points. For Caputo flux and reflecting boundary conditions, the steady-state solution is a constant function. Numerical experiments illustrate the convergence of these numerical methods. Finally, the influence of the reflecting boundary on the steady-state behavior subject to both the Riemann–Liouville and Caputo fluxes is discussed.

1. Introduction

Two-sided fractional diffusion equations replace the second derivative with a weighted average of positive (left) and negative (right) fractional derivatives. The most familiar case is the Riesz derivative, or fractional Laplacian in one dimension, where the weights on the positive and negative fractional derivatives are equal. Two-sided fractional diffusion equations are important in many applications. Benson et al. [7] apply a two-sided fractional diffusion equation to model transport in heterogeneous porous media, in the flow direction. A dataset from Cape Cod is fit using the Riesz fractional derivative, and another dataset from a laboratory sandbox experiment is fit using a model where the weight on the positive fractional derivative is three times larger than the weight on the negative fractional derivative. A more highly heterogeneous dataset from the Macrodispersion Experimental Site in Columbus MS is fit by Benson et al. [8] by a fractional diffusion model with all the weight on the positive fractional derivative. However, Meerschaert, Benson, and Baeumer [31] show that plume spreading transverse to the flow direction follows a two-sided fractional diffusion equation. W. Chen [11] uses the Riesz fractional derivative to model diffusing particles in a turbulent velocity field, and demonstrates the classical Kolmogorov scaling. D. del-Castillo-Negrete, Carreras, and Lynch [14] use the Riesz fractional derivative to model tracer diffusion in plasma turbulence. Mittnik and Rachev [35] apply a symmetric stable model, governed by a Riesz fractional derivative, to high frequency asset returns.

Stable and consistent numerical methods for space fractional diffusion equations and wave equations are necessary for solving many practical problems in turbulence transport models [15], hydrology [33,52], biomedical acoustics [47], and non-

* Corresponding author.
E-mail addresses: kellyja8@stt.msu.edu (J.F. Kelly), mcubed@stt.msu.edu (M.M. Meerschaert).

https://doi.org/10.1016/j.jcp.2018.10.010
0021-9991/

local diffusion/peridynamics [13,16,45] in bounded domains. Most available numerical schemes assume Dirichlet boundary conditions (BCs) [33,34,39]. However, many problems involving space fractional diffusion equations in bounded domains require mass conservation. Dirichlet BCs, which impose a fixed value at the boundary, do not conserve mass. As a result, considerable effort has been spent on developing mass-preserving, *reflecting* (Neumann) BCs for space fractional diffusion equations [5,6,12,19]. In particular, Baeumer et al. [5] proposed explicit Euler schemes for one-sided space fractional diffusion equations in one dimension using either a positive Riemann–Liouville derivative or a positive Patie–Simon derivative in the unit interval, assuming reflecting BCs.

Fractional diffusion using the Riesz derivative in space and a Caputo derivative in time subject to a reflecting boundary condition was discussed by Krepysheva et al. [26] from both a microscopic (particle) and macroscopic (field) perspective. That paper considered symmetric diffusion on a semi-infinite domain. More general continuous time random walks (CTRWs) in a bounded domain were discussed by Burch and Lehoucq [9], while prescribed fractional flux BCs were considered in Zhang et al. [52] from a hydrology perspective. A nonlocal normal derivative was introduced in Dipierro et al. [19] to model reflecting boundaries associated with the two-sided fractional Laplacian.

In this paper, we develop effective numerical methods for two-sided fractional diffusion equations with Neumann or Dirichlet boundary conditions. In Section 2, we formulate the two-sided Riemann–Liouville and Patie–Simon fractional diffusion equations, write both in a conservation form, and develop reflecting and absorbing boundary conditions for these two diffusion equations. In Section 3, we propose explicit and implicit Euler schemes for these diffusion equations, extending the results of Baeumer et al. [5] for the one-sided equations. In Section 4, we prove that the explicit Euler schemes are conditionally stable, and that the implicit Euler schemes are unconditionally stable, using the Gerschgorin circle theorem. In Section 5, we compute the kernels and steady-state solutions for the fractional diffusion equations using both the Riemann–Liouville and Patie–Simon fractional derivatives. Numerical experiments are presented in Section 6, followed by discussion in Section 7 and conclusions in Section 8.

2. Space-fractional diffusion equations

We consider space-fractional diffusion equations with a combination of positive and negative Riemann–Liouville fractional derivatives on a bounded domain $[L, R]$:

$$\frac{\partial}{\partial t}u(x,t) = pC\mathbb{D}^{\alpha}_{L+}u(x,t) + qC\mathbb{D}^{\alpha}_{R-}u(x,t) + s(x,t) \tag{2.1}$$

where $1 < \alpha \le 2$, where $C > 0$ is the diffusion coefficient, $p, q \ge 0$, and $p + q = 1$, while $s(x,t)$ is a source term. The positive and negative Riemann–Liouville derivatives are defined by

$$\mathbb{D}^{\alpha}_{L+}u(x,t) = \frac{\partial^n}{\partial x^n} I^{n-\alpha}_{L+}u(x,t) = \frac{1}{\Gamma(n-\alpha)}\frac{\partial^n}{\partial x^n}\int_L^x \frac{u(y,t)}{(x-y)^{\alpha-n+1}}\,dy \tag{2.2a}$$

$$\mathbb{D}^{\alpha}_{R-}u(x,t) = (-1)^n\frac{\partial^n}{\partial x^n} I^{n-\alpha}_{R-}u(x,t) = \frac{(-1)^n}{\Gamma(n-\alpha)}\frac{\partial^n}{\partial x^n}\int_x^R \frac{u(y,t)}{(y-x)^{\alpha-n+1}}\,dy \tag{2.2b}$$

where $I^{n-\alpha}_{L+}$ and $I^{n-\alpha}_{R-}$ are the positive (left) and negative (right) Riemann–Liouville fractional integrals of order $(n-\alpha)$, respectively, and $n = \lceil\alpha\rceil$ and $\alpha \ne n$. If $\alpha = 2$, then the positive and negative Riemann–Liouville derivatives in (2.1) reduce to the ordinary second derivative. In the symmetric case ($p = q = 1/2$), the symmetric space-fractional diffusion equation

$$\frac{\partial}{\partial t}u(x,t) = \frac{C}{c_\alpha}\frac{\partial^\alpha}{\partial|x|^\alpha}u(x,t) + s(x,t) \tag{2.3}$$

is recovered, where

$$\frac{\partial^\alpha}{\partial|x|^\alpha}u(x,t) = \frac{c_\alpha}{\Gamma(n-\alpha)}\frac{\partial^n}{\partial x^n}\int_L^R \frac{u(y,t)}{|x-y|^{\alpha-1}}\,dy \tag{2.4}$$

is the Riesz derivative (fractional regional Laplacian) defined on a bounded interval [17,27] and $c_\alpha = 1/(2|\cos(\pi\alpha/2)|)$.

We also consider an alternative space-fractional diffusion equation

$$\frac{\partial}{\partial t}u(x,t) = pC\mathbf{D}^{\alpha}_{L+}u(x,t) + qC\mathbf{D}^{\alpha}_{R-}u(x,t) + s(x,t) \tag{2.5}$$

where for $1 < \alpha < 2$

$$\mathbf{D}^{\alpha}_{L+}u(x,t) = \frac{\partial}{\partial x}\partial^{\alpha-1}_{L+}u(x,t) = \frac{1}{\Gamma(2-\alpha)}\frac{\partial}{\partial x}\int_L^x \frac{u'(y,t)}{(x-y)^{\alpha-1}}\,dy \tag{2.6a}$$

$$\mathbf{D}^{\alpha}_{R-}u(x,t) = -\frac{\partial}{\partial x}\partial^{\alpha-1}_{R-}u(x,t) = \frac{1}{\Gamma(2-\alpha)}\frac{\partial}{\partial x}\int_x^R \frac{u'(y,t)}{(y-x)^{\alpha-1}}\,dy \tag{2.6b}$$

are the *Patie–Simon* [37] (also called the *mixed Caputo* [6, Definition 1]) fractional derivatives and

$$\partial^{\alpha}_{L+}u(x,t) = \frac{1}{\Gamma(n-\alpha)}\int_L^x \frac{u^{(n)}(y,t)}{(x-y)^{\alpha-n+1}}\,dy \tag{2.7a}$$

$$\partial^{\alpha}_{R-}u(x,t) = \frac{(-1)^n}{\Gamma(n-\alpha)}\int_x^R \frac{u^{(n)}(y,t)}{(y-x)^{\alpha-n+1}}\,dy \tag{2.7b}$$

are the positive (left) and negative (right) Caputo derivatives [23, Theorem 2.1], respectively.

Remark 2.1. For $1 < \alpha < 2$, the Riemann–Liouville and Patie–Simon derivatives are related via

$$\mathbf{D}^{\alpha}_{L+}u(x,t) = \mathbb{D}^{\alpha}_{L+}u(x,t) - u(L,t)\frac{(x-L)^{-\alpha}}{\Gamma(1-\alpha)} \tag{2.8a}$$

$$\mathbf{D}^{\alpha}_{R-}u(x,t) = \mathbb{D}^{\alpha}_{R-}u(x,t) + u(R,t)\frac{(R-x)^{-\alpha}}{\Gamma(1-\alpha)}, \tag{2.8b}$$

see [5, Equation (6.6)].

2.1. Conservation form

From a physical point of view, $u(x,t)$ may represent the concentration of an ensemble of particles. This concentration is governed by a local mass conservation (continuity) equation

$$\frac{\partial}{\partial t}u(x,t) + \frac{\partial}{\partial x}F(x,t) = 0 \tag{2.9}$$

where $F(x,t)$ is a *flux function* (generalized Fick's law) [15,25,36,44] that accounts for nonlocal diffusion. Comparing (2.9) with (2.1) and (2.5) with no source ($s(x,t) = 0$), the flux function is given by

$$F_{RL}(x,t) = qC\mathbb{D}^{\alpha-1}_{R-}u(x,t) - pC\mathbb{D}^{\alpha-1}_{L+}u(x,t) \tag{2.10a}$$

$$F_C(x,t) = qC\partial^{\alpha-1}_{R-}u(x,t) - pC\partial^{\alpha-1}_{L+}u(x,t) \tag{2.10b}$$

respectively, where $F_{RL}(x,t)$ is a Riemann–Liouville flux and $F_C(x,t)$ is a Caputo flux. Note that $\partial\left[\mathbb{D}^{\alpha-1}_{R-}u(x,t)\right]/\partial x = -\mathbb{D}^{\alpha}_{R-}u(x,t)$ for $1 < \alpha \le 2$. A similar relationship holds for the negative Caputo derivative. The continuity equation (2.9) complemented with either the Riemann–Liouville flux (2.10a) or Caputo flux (2.10b) is the *conservation form*. For traditional diffusion ($\alpha = 2$), both the Riemann–Liouville flux and Caputo flux reduce to the classical Fick's law. An expression similar to (2.10a), written using a pseudo-differential operator on the entire real line, was given in Paradisi et al. [36, Equation (2.5)], while the Caputo flux (2.10b) was proposed for hydrology applications in Zhang et al. [52] (we have corrected a minus sign error in that formula).

Remark 2.2. Both the Riemann–Liouville flux (2.10a) and Caputo flux (2.10b) are nonlocal since the flux at a point x depends on concentration values at locations remote from x. The negative derivatives in (2.10a) and (2.10b) model particle movements from locations to the right of x (negative jumps), while the positive derivatives in (2.10a) and (2.10b) model particle movements from locations to the left of x (positive jumps). Hence, imposing a zero-flux condition is equivalent to balancing these negative and positive particle movements. The Riemann–Liouville flux is the gradient of a sum of fractional integrals, whereas the Caputo flux is the sum of fractionally integrated gradients. Since fractional integration and spatial differentiation do not commute on a bounded interval, the Riemann–Liouville and Caputo fluxes for a given function usually differ. For example, the Caputo flux for a constant function is zero, while the Riemann–Liouville flux of a constant function is non-constant and may be singular at one or more boundary points depending on the weights p and q.

2.2. Reflecting (no-flux) boundary conditions

Using the flux functions defined in (2.10), we can identify a no-flux BC by setting $F(x,t)=0$ at the boundary. Setting $F(x,t)=0$ at $x=L$ and $x=R$ in (2.10) yields reflecting BCs:

$$\text{RL: } p\mathbb{D}_{L+}^{\alpha-1}u(x,t)=q\mathbb{D}_{R-}^{\alpha-1}u(x,t) \text{ for } x=L \text{ and } x=R \text{ for all } t\ge 0 \tag{2.11a}$$

$$\text{C: } p\partial_{L+}^{\alpha-1}u(x,t)=q\partial_{R-}^{\alpha-1}u(x,t) \text{ for } x=L \text{ and } x=R \text{ for all } t\ge 0. \tag{2.11b}$$

These boundary conditions are *nonlocal* since the BC at $x=L$ or $x=R$ depends on all values of $u(x,t)$ in the interval $[L,R]$. By Remark 2.2, these boundary conditions impose a balance of negative and positive particle movements.

The special case $p=1$ was considered in Baeumer et al. [5], yielding the no-flux BC

$$\text{RL: } \mathbb{D}_{L+}^{\alpha-1}u(x,t)=0 \text{ for } x=L \text{ and } x=R \text{ for all } t\ge 0 \tag{2.12a}$$

$$\text{C: } \partial_{L+}^{\alpha-1}u(x,t)=0 \text{ for } x=L \text{ and } x=R \text{ for all } t\ge 0. \tag{2.12b}$$

For the special case $q=1$, the positive Riemann–Liouville and Caputo derivatives $\mathbb{D}_{L+}^{\alpha-1}$ and $\partial_{L+}^{\alpha-1}$ are replaced by the negative Riemann–Liouville and Caputo derivatives $\mathbb{D}_{R-}^{\alpha-1}$ and $\partial_{R-}^{\alpha-1}$, respectively. In the symmetric (fractional Laplacian) case $p=q$, we have

$$\text{RL: } \mathbb{D}_{L+}^{\alpha-1}u(x,t)=\mathbb{D}_{R-}^{\alpha-1}u(x,t) \text{ for } x=L \text{ and } x=R \text{ for all } t\ge 0 \tag{2.13a}$$

$$\text{C: } \partial_{L+}^{\alpha-1}u(x,t)=\partial_{R-}^{\alpha-1}u(x,t) \text{ for } x=L \text{ and } x=R \text{ for all } t\ge 0. \tag{2.13b}$$

Unlike the one-sided cases, reflecting boundary conditions for the symmetric diffusion equation involves a *balance* of two fractional derivatives of order $(\alpha-1)$.

2.3. Reflecting/absorbing, absorbing/reflecting, and absorbing BCs

We also consider reflecting on the left boundary and absorbing on the right boundary (reflecting/absorbing BCs)

$$\text{RL: } p\mathbb{D}_{L+}^{\alpha-1}u(x,t)=q\mathbb{D}_{R-}^{\alpha-1}u(x,t) \text{ for } x=L \text{ and } u(R,t)=0 \text{ for all } t\ge 0 \tag{2.14a}$$

$$\text{C: } p\partial_{L+}^{\alpha-1}u(x,t)=q\partial_{R-}^{\alpha-1}u(x,t) \text{ for } x=L \text{ and } u(R,t)=0 \text{ for all } t\ge 0, \tag{2.14b}$$

and absorbing on the left and reflecting on the right (absorbing/reflecting BCs)

$$\text{RL: } u(L,t)=0 \text{ and } p\mathbb{D}_{L+}^{\alpha-1}u(x,t)=q\mathbb{D}_{R-}^{\alpha-1}u(x,t) \text{ for } x=R \text{ for all } t\ge 0 \tag{2.15a}$$

$$\text{C: } u(L,t)=0 \text{ and } p\partial_{L+}^{\alpha-1}u(x,t)=q\partial_{R-}^{\alpha-1}u(x,t) \text{ for } x=R \text{ for all } t\ge 0. \tag{2.15b}$$

The special case of $p=1$ and $q=0$ of these BCs was considered in Baeumer et al. [5]. Absorbing (Dirichlet) BCs on both boundaries $u(L,t)=u(R,t)=0$ will also be considered.

2.4. Conservation of mass

The no-flux (reflecting) BCs given by (2.11) imply that the total mass is conserved. Given a linear operator A on the Banach space $X=L^1[L,R]$, the domain $\mathrm{Dom}(A)$ is the set of $f\in X$ for which Af exists in X. For the operators considered in the Proposition below, we assume that the Cauchy problem $\frac{\partial}{\partial t}u=Au$ has a strong solution for any initial condition $u_0\in\mathrm{Dom}(A)$.

Proposition 2.3. *Let $M_0=\int_L^R u(x,t)\,dx$ be the total mass and let $\mathcal{D}_{RL}^{\alpha}=pC\mathbb{D}_{L+}^{\alpha}+qC\mathbb{D}_{R-}^{\alpha}$ and $\mathcal{D}_{PS}^{\alpha}=pC\mathbf{D}_{L+}^{\alpha}+qC\mathbf{D}_{R-}^{\alpha}$ be the fractional operators on the right-hand side of (2.1) and (2.5), respectively, with $s(x,t)=0$ and reflecting boundary condition (2.11a) or (2.11b), respectively. Let $\mathrm{Dom}(\mathcal{D}_{RL}^{\alpha})$ and $\mathrm{Dom}(\mathcal{D}_{PS}^{\alpha})$ be the domains of $\mathcal{D}_{RL}^{\alpha}$ and $\mathcal{D}_{PS}^{\alpha}$, respectively. Given a non-negative initial condition $u(x,0)=u_0(x)\in\mathrm{Dom}(\mathcal{D}_{RL}^{\alpha})$ for (2.1) or $u(x,0)=u_0(x)\in\mathrm{Dom}(\mathcal{D}_{PS}^{\alpha})$ for (2.5), the total mass is conserved.*

Proof. Using the definition of the generator for the corresponding C_0 semigroups on the Banach space $L^1(L,R)$ [32, Section 3.3], the time derivative may be moved inside the integral

$$\frac{\partial M_0}{\partial t}=\int_L^R \frac{\partial}{\partial t}u(x,t)\,dx=\int_L^R \mathcal{D}^{\alpha}u(x,t)\,dx,$$

where $\mathcal{D}^{\alpha}=\mathcal{D}_{RL}^{\alpha}$ or $\mathcal{D}_{PS}^{\alpha}$. Then apply the conservation form (2.9),

$$\frac{\partial M_0}{\partial t} = -\int_L^R \frac{\partial}{\partial x} F(x,t)\,dx$$
$$= F(L,t) - F(R,t).$$

Since $F(L,t) = F(R,t) = 0$ for all t by (2.12), $\partial M_0/\partial t = 0$ and $M_0 = \int_L^R u_0(x)\,dx$ for all $t \geq 0$. □

Remark 2.4. Note that a zero-flux boundary condition is a sufficient, but not necessary condition for mass conservation. A more general condition is $F(L,t) = F(R,t)$, where the flux leaving the right boundary re-enters the domain at the left boundary (and vice versa).

Remark 2.5. It is also interesting to consider fractional boundary value problems in higher dimensions. Gunzburger et al. [24] model turbulent flows using a modified Navier–Stokes equation, where the diffusive operator is replaced by a fractional Laplacian. Epps and Cushman-Roisin [20] use a generalized Boltzmann kinetic theory to derive a fractional Laplacian term for the mean friction force arising in a turbulent flow in three dimensions. Viswanathan et al. [50] model the flight of the Albatross using a fractional Laplacian in two dimensions. Lischke et al. [27] provide a review of the fractional Laplacian, and numerical methods for Dirichlet boundary value problems. At present, the formulation of the corresponding Neumann problem for the vector fractional Laplacian is an area of active research. However, in certain cases, the results of this paper can be applied in higher dimensions. Consider the vector fractional diffusion equation

$$\frac{\partial}{\partial t} u(\boldsymbol{x},t) = \sum_{i=1}^{d} \left[p_i C_i \frac{\partial^\alpha}{\partial x_i^\alpha} u(\boldsymbol{x},t) + q_i C_i \frac{\partial^\alpha}{\partial(-x_i)^\alpha} u(\boldsymbol{x},t) \right] + s(\boldsymbol{x},t) \tag{2.16}$$

where the vector $\boldsymbol{x} = (x_1, \ldots, x_d)$ and $p_i + q_i = 1$ for $1 \leq i \leq d$. If we consider the boundary value problem on a rectangle, we can apply absorbing or reflecting boundary conditions in each dimension, in the forms considered in this paper. Details will be included in a follow-up paper.

3. Finite-difference approximations

To discretize (2.1), we can use either an explicit or implicit Euler scheme combined with the shifted Grünwald estimate [34]:

$$\mathbb{D}_{L+}^{\alpha} f(x_j) = h^{-\alpha} \sum_{i=0}^{j+1} g_i^\alpha f\left(x_{j-i+1}\right) + \mathcal{O}(h) \tag{3.1a}$$

$$\mathbb{D}_{R-}^{\alpha} f(x_j) = h^{-\alpha} \sum_{i=0}^{n-j+1} g_i^\alpha f\left(x_{j+i-1}\right) + \mathcal{O}(h) \tag{3.1b}$$

where $h = (R-L)/n$ is the grid spacing, $x_j = L + hj$ are the $n+1$ grid points, and

$$g_i^\alpha = \frac{(-1)^i \Gamma(\alpha+1)}{\Gamma(i+1)\Gamma(\alpha-i+1)} \tag{3.2}$$

are the Grünwald weights [32, Equation (2.4)]. The resulting explicit Euler scheme is given by

$$u\left(x_j, t_{k+1}\right) = u\left(x_j, t_k\right) + \frac{pC\Delta t}{h^\alpha} \sum_{i=0}^{j+1} g_i^\alpha u\left(x_{j-i+1}, t_k\right) + \frac{qC\Delta t}{h^\alpha} \sum_{i=0}^{n-j+1} g_i^\alpha u\left(x_{j+i-1}, t_k\right) + \Delta t s\left(x_j, t_k\right). \tag{3.3}$$

Defining a row vector containing the solution at time $t_k = k\Delta t$ via $\mathbf{u}_k = [u(x_i, t_k)]$ along with the source $\mathbf{s}_k = [\Delta t\, s(x_i, t_k)]$ yields

$$\mathbf{u}_{k+1} = \mathbf{u}_k + \beta_+ \mathbf{u}_k B^+ + \beta_- \mathbf{u}_k B^- + \mathbf{s}_k \tag{3.4}$$

where $\beta_+ = pCh^{-\alpha}\Delta t$, $\beta_- = qCh^{-\alpha}\Delta t$, and $B^\pm$ are $(n+1)\times(n+1)$ iteration matrices, which will be written explicitly below. These iteration matrices depend upon both the flux function and the boundary conditions. The explicit scheme (3.4) may be written compactly as

$$\mathbf{u}_{k+1} = \mathbf{u}_k A + \mathbf{s}_k \tag{3.5}$$

where $A = I + \beta_+ B^+ + \beta_- B^-$.

Applying an implicit Euler discretization to (2.1) yields

$$\mathbf{u}_{k+1} = \mathbf{u}_k + \beta_+ \mathbf{u}_{k+1} B^+ + \beta_- \mathbf{u}_{k+1} B^- + \mathbf{s}_{k+1}, \tag{3.6}$$

where $B^\pm$ are the same iteration matrices utilized in (3.4). This implicit scheme may be written as

$$\mathbf{u}_{k+1} M = \mathbf{u}_k + \mathbf{s}_{k+1}, \tag{3.7}$$

where $M = I - \beta_+ B^+ - \beta_- B^-$. The discretization of (2.5) leads to the same iteration equations (3.5) and (3.7), but with a slightly different iteration matrix, which will be written explicitly below.

3.1. Iteration matrices: Riemann–Liouville flux

We first consider the explicit and implicit Euler schemes associated with (2.1) subject to reflecting BCs. The entries of B^+ are given by [5, Equation 4.2]

$$b_{i,j} = \begin{cases} g^{\alpha}_{j-i+1} & \text{if } 0 < j < n \text{ and } i \le j+1 \\ 1 & \text{if } i = 1 \text{ and } j = 0 \\ 1-\alpha & \text{if } i = j = 0 \\ -g^{\alpha-1}_{n-i} & \text{if } j = n \text{ and } i \le n \\ 0 & \text{otherwise.} \end{cases} \tag{3.8}$$

The entries for column $j = 0$ prevent mass from leaving the left boundary $x = L$, while the entries for $j = n$ prevent mass from leaving the right boundary $x = R$. The fraction of mass that would otherwise leave the domain is deposited at the boundary, thereby modeling *inelastic* collisions at $x = L$ and $x = R$. Comparing the second and third terms in (3.3), we see that the entries of B^- associated with the negative Riemann–Liouville fractional derivative are $[b_{n-i,n-j}]$.

Next, consider the reflecting/absorbing BCs given by (2.14a). The iteration matrix B^{ra+} for the one-sided Riemann–Liouville derivative with these BCs is simply (3.8) with all entries in column $j = n$ set equal to zero. The iteration matrix B^{ar+} for the one-sided Riemann–Liouville derivative with absorbing/reflecting BCs (2.15a) is (3.8) with all entries in column $j = 0$ set equal to zero. Finally, the iteration matrix B^{aa+} for the one-sided Riemann–Liouville derivative with absorbing BCs $u(L,t) = u(R,t) = 0$ is (3.8) with all entries in both columns $j = 0$ and $j = n$ set equal to zero. Comparing the second and third terms in (3.3), we see that replacing i and j by $n - i$ and $n - j$ reverses the roles for r and a. Hence, the entries of B^{ra-}, B^{ar-}, and B^{aa-} are simply $b^{ar}_{n-i,n-j}$, $b^{ra}_{n-i,n-j}$, and $b^{aa}_{n-i,n-j}$, respectively.

3.2. Iteration matrices: Caputo flux

In Section 6 of [5], an explicit Euler scheme was proposed to solve (2.5) in the special case $q = 0$ subject to Dirichlet (absorbing) and Neumann (reflecting) BCs. Absorbing/reflecting and reflecting/absorbing BCs were also considered. For reflecting BCs (2.11b), the iteration matrix $B = \left[b_{i,j}\right]$ is given by [5, Equation 6.11]

$$b_{i,j} = \begin{cases} g^{\alpha}_{j-i+1} & \text{if } 0 < j < n \text{ and } i \le j+1 \\ 1 & \text{if } i = 1 \text{ and } j = 0 \\ -1 & \text{if } i = j = 0 \\ -g^{\alpha-1}_{j} & \text{if } i = 0 \text{ and } 0 < j < n \\ -g^{\alpha-2}_{n-1} & \text{if } i = 0 \text{ and } j = n \\ -g^{\alpha-1}_{n-i} & \text{if } j = n \text{ and } 0 < i \le n \\ 0 & \text{otherwise,} \end{cases} \tag{3.9}$$

and then the entries of B^- are $\left[b_{n-i,n-j}\right]$. As in the Riemann–Liouville flux case, the iteration matrices for reflecting/absorbing and absorbing/reflecting BCs are simply (3.9) with all entries in the n-th column or zeroth column set to zero, respectively [5, Equations 6.15 and 6.17]. Finally, for absorbing BCs $u(L,t) = u(R,t) = 0$, the iteration matrix is given by (3.9) with all entries in columns $j = 0$ and $j = n$ set to zero.

3.3. Consistency of boundary conditions

In this subsection, we show that the iteration matrices (3.8) and (3.9) are consistent with the reflecting boundary conditions (2.11a) and (2.11b), respectively, as $h \to 0$ and $\Delta t \to 0$. We restrict our attention to the explicit Euler scheme since the argument for implicit Euler is identical. Assuming no source term, the update equation for either diffusion equation at the right boundary $j = n$ is

$$u\left(x_n, t_{k+1}\right) = u\left(x_n, t_k\right) + \beta_+ \sum_{i=0}^{n} b_{i,n} u\left(x_i, t_k\right) + \beta_- \sum_{i=0}^{n} b_{n-i,0} u\left(x_i, t_k\right) \tag{3.10}$$

First, consider the iteration matrix for the explicit Euler schemes associated with the space-fractional diffusion equation using Riemann–Liouville flux (2.1). Evaluating (3.10) yields

$$u\left(x_n, t_{k+1}\right) = u\left(x_n, t_k\right) - \frac{pC\Delta t}{h^\alpha} \sum_{i=0}^{n} g_{n-i}^{\alpha-1} u\left(x_i, t_k\right) + \frac{qC\Delta t}{h^\alpha}\left(u\left(x_{n-1}, t_k\right) + (1-\alpha) u\left(x_n, t_k\right)\right),$$

which is equivalent to

$$h \frac{u\left(x_n, t_{k+1}\right) - u\left(x_n, t_k\right)}{\Delta t} = -\frac{pC}{h^{\alpha-1}} \sum_{i=0}^{n} g_{n-i}^{\alpha-1} u\left(x_i, t_k\right) + \frac{qC}{h^{\alpha-1}} \sum_{i=0}^{1} g_i^{\alpha-1} u\left(x_{n+i-1}, t_k\right).$$

The first term on the right hand side is just the Grünwald approximation of $D_{L+}^{\alpha-1} u(x, t_k)$ at $x = R$ multiplied by $-pC$, while the second term is the Grünwald approximation of $D_{R-}^{\alpha-1} u(x, t_k)$ at $x = R$ multiplied by qC. As $h \to 0$, the Grünwald approximation of $D_{L+}^{\alpha-1} u(x, t_k)$ is consistent with (2.2a) at $x = R$ in both the L^1 and supremum norms [4, Theorem 3.3]. For additional details regarding the second term, see [6, Proposition 19]. As $\Delta t \to 0$ and $h \to 0$, the left hand side approaches zero, yielding $p\mathbb{D}_{L+}^{\alpha-1} u(x, t) = q\mathbb{D}_{R-}^{\alpha-1} u(x, t)$ at $x = R$. Writing out the update equation at the left boundary $j = 0$ and performing a similar argument yields the same boundary condition at $x = L$.

Now consider the space-fractional diffusion equation using Caputo flux (2.5). Applying (3.10) yields

$$u\left(x_n, t_{k+1}\right) = u\left(x_n, t_k\right) - \frac{pC\Delta t}{h^\alpha}\left(-g_{n-1}^{\alpha-2} u\left(x_0, t_k\right) - \sum_{i=1}^{n} g_{n-i}^{\alpha-1} u\left(x_i, t_k\right)\right) + \frac{qC\Delta t}{h^\alpha}\left(u\left(x_{n-1}, t_k\right) - u\left(x_n, t_k\right)\right).$$

Applying the identity $g_n^\alpha - g_n^{\alpha-1} = -g_{n-1}^{\alpha-1}$ [5, Equation (6.9)] and rearranging yields

$$\begin{aligned} & h \frac{u\left(x_n, t_{k+1}\right) - u\left(x_n, t_k\right)}{\Delta t} \\ & \quad = -\frac{pC}{h^{\alpha-1}}\left(\sum_{i=0}^{n} g_{n-i}^{\alpha-1} u\left(x_i, t_k\right) - g_n^{\alpha-2} u\left(x_0, t_k\right)\right) + \frac{qC}{h^{\alpha-1}}\left(\sum_{i=0}^{1} g_i^{\alpha-1} u\left(x_{n+i-1}, t_k\right) - g_1^{\alpha-2} u\left(x_n, t_k\right)\right). \end{aligned}$$

The first term on the right hand side is the Grünwald approximation of $\partial_{L+}^{\alpha-1} u(x, t_k)$ multiplied by $-pC$ at $x = R$, while the second term is the Grünwald approximation of $\partial_{R-}^{\alpha-1} u(x, t_k)$ at $x = R$ multiplied by qC [6, Section 6]. Let $\Delta t \to 0$, yielding $p\partial_{L+}^{\alpha-1} u(x, t) = q\partial_{R-}^{\alpha-1} u(x, t)$ at $x = R$. Applying a similar argument to the update equation at the left boundary $j = 0$ yields the same boundary condition at $x = L$.

4. Stability analysis

4.1. Riemann–Liouville flux

To prove conditional stability of the explicit Euler scheme (3.5) and unconditional stability of the implicit Euler scheme (3.7), we estimate the eigenvalues of the matrices A and M using the Gerschgorin circle theorem [3, Theorem 9.1]. The following Lemma is used.

Lemma 4.1. *The radii of the Gerschgorin circles of the matrix $B^+ = [b_{i,j}]$ given by (3.8)*

$$r_i = \sum_{j=0, j \neq i}^{n} \left|b_{i,j}\right| \tag{4.1}$$

are given by

$$r_i = \begin{cases} \alpha - 1 & \text{if } i = 0 \\ \alpha & \text{if } 0 < i < n \\ 1 & \text{if } i = n, \end{cases} \tag{4.2}$$

while the radii of the Gerschgorin circles of the matrix $B^- = [b_{n-i,n-j}]$ are r_{n-j}.

Proof. Using (3.2) we can see that $g_0^\alpha = 1$, $g_1^\alpha = -\alpha$, $g_i^\alpha > 0$ for all $i > 1$, $g_0^{\alpha-1} = 1$, and $g_i^{\alpha-1} < 0$ for all $i > 0$. Hence all the off-diagonal entries in both B^+ and B^- are non-negative, allowing us to neglect the absolute value in (4.1). Then write

$$\begin{aligned} r_0 =& \sum_{j=1}^{n-1} g_{j+1}^\alpha - g_n^{\alpha-1} \\ =& \sum_{j=2}^{n} g_j^\alpha - g_n^{\alpha-1} \\ =& g_n^{\alpha-1} - 1 + \alpha - g_n^{\alpha-1} \\ =& \alpha - 1 \end{aligned}$$

where we used [43, Equation 20.4]

$$\sum_{j=0}^{n} g_j^\alpha = g_n^{\alpha-1}. \tag{4.3}$$

Next, consider rows $0 < i < n$:

$$\begin{aligned} r_i =& 1 + \sum_{j=i+1}^{n-1} g_{j-i+1}^\alpha - g_{n-i}^{\alpha-1} \\ =& 1 + \sum_{j=2}^{n-i} g_j^\alpha - g_{n-i}^{\alpha-1} \\ =& 1 - 1 + \alpha + g_{n-i}^{\alpha-1} - g_{n-i}^{\alpha-1} \\ =& \alpha. \end{aligned}$$

For row $i = n$, we have $r_n = 1$ since there is only one off-diagonal entry. Finally, the radii of the Gerschgorin circles of the matrix B^- are

$$\sum_{j=0,\, j\neq i}^{n} b_{n-i,n-j} = \sum_{j=0,\, j\neq n-i}^{n} b_{n-i,j} = r_{n-i},$$

completing the proof. □

Remark 4.2. The Gerschgorin radii associated with B^{ar+}, B^{ra+}, and B^{aa+} are less than or equal to the radii of B^+ since the entries of B^{ar+}, B^{ra+}, and B^{aa+} are either those of B^+ or zero. The same is true for B^{ar-}, B^{ra-}, and B^{aa-}.

Proposition 4.3. *The explicit Euler method (3.4) for (2.1) subject to any combination of absorbing and reflecting BCs is stable if $\Delta t/h^\alpha \le 1/(\alpha C)$ over the region $L \le x \le R$ and $0 \le t \le T$.*

Proof. First consider the case of reflecting BCs. By the Gerschgorin circle theorem [3, Theorem 9.1], it suffices to show the eigenvalues of A are inside the closed unit disk. Using (4.2), the radii of the Gerschgorin circles for the matrix A are given by

$$R_i = \begin{cases} \beta_+(\alpha-1) + \beta_- & \text{if } i = 0 \\ \beta_+\alpha + \beta_-\alpha & \text{if } 0 < i < n \\ \beta_+ + \beta_-(\alpha-1) & \text{if } i = n, \end{cases} \tag{4.4}$$

while the diagonal entries of A are

$$a_{i,i} = \begin{cases} 1 - \beta_+(\alpha-1) - \beta_- & \text{if } i = 0 \\ 1 - (\beta_+ + \beta_-)\alpha & \text{if } 0 < i < n \\ 1 - \beta_+ - \beta_-(\alpha-1) & \text{if } i = n. \end{cases} \tag{4.5}$$

Hence $a_{i,i} + R_i = 1$ for all i, while $a_{i,i} - R_{i,i} = 1 - 2R_i$. To ensure $|\lambda_i| \le 1$ and stability, we require $1 - 2R_i \ge -1$, or $R_i \le 1$. Since the largest R_i is $\alpha(\beta_+ + \beta_-)$, we require

$$\alpha(\beta_+ + \beta_-) \leq 1,$$

which is true by hypothesis. The cases of absorbing/reflecting, reflecting/absorbing, and absorbing BCs are similar, using Remark 4.2. □

Remark 4.4. The same explicit stability condition was shown for the fractional diffusion equation with Dirichlet BCs in [34]. For the case of $\alpha = 2$ with a diffusion coefficient $C = 1$, we recover the well-known stability constraint for the diffusion equation with both Dirichlet (absorbing) and Neumann (reflecting) BCs [41]:

$$\beta = \frac{\Delta t}{h^2} \leq \frac{1}{2}. \tag{4.6}$$

For the case of $\alpha = 1$ and $C = 1$, we recover the stability constraint for the transport equation with both Dirichlet (absorbing) and Neumann (reflecting) BCs:

$$\beta = \frac{\Delta t}{h} \leq 1. \tag{4.7}$$

Proposition 4.5. *The implicit Euler method for (2.1) subject to any combination of absorbing and reflecting BCs for $1 < \alpha \leq 2$ is unconditionally stable for all Δt and any grid spacing h.*

Proof. As in the explicit scheme proof, we use [3, Theorem 9.1]. First, note that the off-diagonal entries $m_{i,j}$ of M are simply $-\beta_+ b_{i,j} - \beta_- b_{n-i,n-j}$. Hence, the radii of the Gerschgorin circles for the matrix M are also given by (4.4), while the diagonal entries of M are

$$m_{i,i} = \begin{cases} 1 + \beta_+(\alpha - 1) + \beta_- & \text{if } i = 0 \\ 1 + (\beta_+ + \beta_-)\alpha & \text{if } 0 < i < n \\ 1 + \beta_+ + \beta_-(\alpha - 1) & \text{if } i = n. \end{cases} \tag{4.8}$$

The complex absolute values of the eigenvalues λ_i of M are bounded by $m_{i,i} - R_i \leq |\lambda_i| \leq m_{i,i} + R_i$. Clearly, $m_{i,i} - R_i = 1$ for all $0 \leq i \leq n$, while $m_{i,i} + R_i = 1 + 2R_{i,i} > 1$. Hence, $|\lambda_i| \geq 1$, implying that every eigenvalue of the inverse matrix M^{-1} has complex absolute values less than or equal to 1. The proof for other combinations of BCs is similar. □

4.2. Caputo flux

In this section, we prove stability of the explicit and implicit Euler schemes for (2.5).

Lemma 4.6. *The radii of the Gerschgorin circles of the matrices B^+ and B^- with entries specified by (3.9) and $\left[b_{n-i,n-j}\right]$, respectively, are given by*

$$r_i = \begin{cases} 1 & \textit{if } i = 0 \textit{ or } i = n \\ \alpha & \textit{if } 0 < i < n. \end{cases} \tag{4.9}$$

Proof. Again, note that all the off-diagonal entries are positive. First, consider row $i = 0$:

$$\begin{aligned} r_0 = &-\sum_{j=1}^{n-1} g_j^{\alpha-1} + g_{n-1}^{\alpha-2} \\ =&1 - \sum_{j=0}^{n-1} g_j^{\alpha-1} + g_{n-1}^{\alpha-2} \\ =&1 - g_{n-1}^{\alpha-2} + g_{n-1}^{\alpha-2} = 1, \end{aligned}$$

where (4.3) is used in the third line. Next, consider rows $0 < i < n$:

$$\begin{aligned} r_i =&1 + \sum_{j=i+1}^{n-1} g_{j-i+1}^{\alpha} - g_{n-i}^{\alpha-1} \\ =&1 + \sum_{j=2}^{n-i} g_j^{\alpha} - g_{n-i}^{\alpha-1} \\ =&1 - 1 + \alpha + g_{n-i}^{\alpha-1} - g_{n-i}^{\alpha-1} = \alpha. \end{aligned}$$

Finally, if $i = n$, then there is a single entry $r_n = -g_0^{\alpha-1} = 1$. Since B^- has entries $[b_{n-i,n-j}]$ and $r_0 = r_n = 1$, it follows that B^- also has Gerschgorin radii given by (4.9). □

Proposition 4.7. *The explicit Euler method for (2.5) subject to any combination of absorbing and reflecting BCs is stable if $\Delta t/h^\alpha \leq 1/(\alpha C)$ over the region $L \leq x \leq R$ and $0 \leq t \leq T$.*

Proof. As with (4.3), we consider the case of reflecting BCs. Note that

$$a_{i,i} = \begin{cases} 1-(\beta_+ + \beta_-) & \text{if } i=0 \text{ or } i=n \\ 1-(\beta_+ + \beta_-)\alpha & \text{if } 0<i<n, \end{cases}$$

with Gerschgorin radii given by (4.10). Hence, $a_{i,i} + R_i = 1$ for all i and we require $R_i \leq 1$ to bound all eigenvalues in the unit disk. Hence, $\alpha\,(\beta_+ + \beta_-) \leq 1$, which is satisfied by hypothesis. The other three cases are similar since the Gerschogorin radii are bounded above by (4.9). □

Proposition 4.8. *The implicit Euler scheme for (2.5) subject to any combination of absorbing and reflecting BCs for $1 < \alpha \leq 2$ is unconditionally stable for all Δt.*

Proof. Using (4.9), the radii of the Gerschgorin circles for the matrix M with reflecting BCs are given by

$$R_i = \begin{cases} (\beta_+ + \beta_-) & \text{if } i=0 \text{ or } i=n \\ \alpha\,(\beta_+ + \beta_-) & \text{if } 0<i<n, \end{cases} \tag{4.10}$$

while the diagonal entries of M are

$$m_{i,i} = \begin{cases} 1+(\beta_+ + \beta_-) & \text{if } i=0 \text{ or } i=n \\ 1+(\beta_+ + \beta_-)\alpha & \text{if } 0<i<n. \end{cases}$$

Hence, $m_{i,i} - R_i = 1$, while $m_{i,i} + R_i = 1 + 2R_i \geq 1$. Application of the Gerschgorin theorem places all eigenvalues of M in the set $|\lambda_i| \geq 1$, implying that the spectral radius of M^{-1} is less than or equal to one. The proof with other combinations of BCs is similar. □

5. Steady-state solutions

In this section, we compute the steady-state solutions $u_\infty(x)$ that satisfy (2.1) and (2.5), and particular steady-state solutions that satisfy reflecting (no-flux) BCs. We first compute the kernel (null-space) of the two-sided Riemann–Liouville and Patie–Simon derivatives, and then construct steady-state solutions that satisfy reflecting BCs using functions in the kernel.

5.1. Riemann–Liouville flux

In the one-sided case ($p = 1$), the kernel (null-space) of the Riemann–Liouville derivative on the interval $[-1, 1]$ was computed in Baeumer et al. [6]

$$\ker\left(\mathbb{D}^\alpha_{-1^+}\right) = c_0(x+1)^{\alpha-2} + c_1(x+1)^{\alpha-1}, \tag{5.1}$$

where c_0 and c_1 are arbitrary constants. The only steady state solution with a total mass of one that satisfies reflecting BCs is $u_\infty(x) = 2^{1-\alpha}(\alpha-1)(1+x)^{\alpha-2}$, which is singular at the left end-point $x = -1$ and regular at the right end-point $x = 1$. To check (5.1), note that since the Riemann–Liouville derivative (2.2a) is the second derivative of the $2-\alpha$ Riemann–Liouville integral, the Riemann–Liouville derivative of a function can be identically zero if and only if the $2-\alpha$ Riemann–Liouville integral is linear. Then apply the Riemann–Liouville integral of order $2-\alpha$ to both terms, which yields a linear function in x. The second derivative of this expression is identically zero. A similar argument holds for the one-sided negative case ($q = 1$), yielding $u_\infty(x) = 2^{1-\alpha}(\alpha-1)(1-x)^{\alpha-2}$, which is regular at $x = -1$ and singular at $x = 1$.

In this section, we derive the steady-state solution of (2.1) with $s = 0$ on the interval $[-1, 1]$

$$p\mathbb{D}^\alpha_{-1^+}u_\infty(x) + q\mathbb{D}^\alpha_{1^-}u_\infty(x) = 0 \tag{5.2}$$

subject to a reflecting BC at both boundaries:

$$p\mathbb{D}^{\alpha-1}_{-1^+}u_\infty(x) = q\mathbb{D}^{\alpha-1}_{1^-}u_\infty(x) \text{ for } x = -1 \text{ and } 1. \tag{5.3}$$

The kernel and steady state solution may be derived using the method of orthogonal polynomials [2,40], see also [38, Section 6.4].

Definition 5.1. The Jacobi polynomials $P_m^{\mu,\nu}(x)$ of order $m \geq 0$ are m-th degree polynomials orthogonal with respect to the weight $(1-x)^\mu(1+x)^\nu$ on the interval $[-1,1]$, where $\mu, \nu > -1$. These polynomials may be defined via [1, Equation (22.3.2)]

$$P_m^{\mu,\nu}(x) = \frac{\Gamma(\mu+m+1)}{m!\Gamma(\mu+\nu+m+1)} \sum_{k=0}^{m} \binom{m}{k} \frac{\Gamma(\mu+\nu+m+k+1)}{2^k\Gamma(\mu+k+1)}(x-1)^k. \tag{5.4}$$

In particular, $P_0^{\mu,\nu}(x) = 1$ and $P_1^{\mu,\nu}(x) = (\mu+\nu+2)x/2 + (\mu-\nu)/2$.

Definition 5.2. The two-sided Jacobi polyfractonomials used by Mao and Karniadakis [30] $Q_m^{\mu,\nu}(x)$ are defined by

$$Q_m^{\mu,\nu}(x) = (1-x)^\mu(1+x)^\nu P_m^{\mu,\nu}(x) \tag{5.5}$$

where $P_m^{\mu,\nu}(x)$ is defined by (5.4).

An identity involving $Q_m^{\mu,\nu}(x)$ and the two-sided fractional integral is given by Podlubny [38, Theorem 6.4] with $r = 0$ and $k = -1$:

$$\int_{-1}^{1} \left(\cos(\gamma\pi)\,\mathrm{sgn}(x-t) + \frac{\sin(\pi\gamma)}{\tan(\tilde{\nu}\pi/2)} \right) \frac{Q_m^{-\gamma+\tilde{\nu}/2,\gamma+\tilde{\nu}/2-1}(t)}{|x-t|^{\tilde{\nu}}}\,dt = A_m P_m^{\gamma+\tilde{\nu}/2-1,-\gamma+\tilde{\nu}/2}(x), \tag{5.6}$$

where $0 < \tilde{\nu} < 1$, $0 < \gamma < 1$, and

$$A_m = \frac{\pi\Gamma(m+\tilde{\nu})}{m!\Gamma(\tilde{\nu})\sin(\tilde{\nu}\pi/2)}. \tag{5.7}$$

Using (5.6), we will characterize the kernel $\ker(\mathcal{D}_{RL}^{\alpha})$ of the two-sided Riemann–Liouville derivative. First, we need a technical lemma.

Lemma 5.3. *Let $1 < \alpha < 2$, $p + q = 1$, and let $m \geq 0$ be an integer. Then*

$$pI_{-1^+}^{2-\alpha} Q_m^{\mu,\nu}(x) + qI_{1^-}^{2-\alpha} Q_m^{\mu,\nu}(x) = C_m P_m^{\nu,\mu}(x) \tag{5.8}$$

where $I_{-1^+}^{2-\alpha}$ and $I_{1^-}^{2-\alpha}$ are the positive and negative Riemann–Liouville fractional integrals of order $(2-\alpha)$, respectively, and

$$\mu + \nu = \alpha - 2 \tag{5.9a}$$

$$p - q = \cot\left(\pi\left(\frac{\alpha-1}{2} - \mu\right)\right)\tan\left(\frac{\alpha-1}{2}\pi\right) \tag{5.9b}$$

$$C_m = \frac{\sin(\pi(\alpha-1)/2)\Gamma(m+\alpha-1)}{m!\sin(\pi(\alpha-1)/2 - \pi\mu)}. \tag{5.9c}$$

Proof. In (5.6), let $W_\pm = \pm\cos(\pi\gamma) + \sin(\pi\gamma)/\tan(\tilde{\nu}\pi/2)$, $\tilde{\nu} = \alpha - 1$, and define

$$\mu = -\gamma + \frac{\alpha-1}{2} \tag{5.10a}$$

$$\nu = \gamma - 1 + \frac{\alpha-1}{2}. \tag{5.10b}$$

Split (5.6) into two terms and divide both sides by $\Gamma(2-\alpha)$, yielding

$$W_+ I_{-1^+}^{2-\alpha} Q_m^{\mu,\nu}(x) + W_- I_{1^-}^{2-\alpha} Q_m^{\mu,\nu}(x) = \frac{A_m}{\Gamma(2-\alpha)} P_m^{\nu,\mu}(x). \tag{5.11}$$

By the Euler reflection formula $\Gamma(2-\alpha)\Gamma(\alpha-1) = \pi/\sin(\pi(\alpha-1))$ and the double angle formula for the sine,

$$\tilde{A}_m = \frac{A_m}{\Gamma(2-\alpha)} = \frac{2\Gamma(m+\alpha-1)\cos((\alpha-1)\pi/2)}{m!}, \tag{5.12}$$

yielding

$$W_+ I_{-1^+}^{2-\alpha} Q_m^{\mu,\nu}(x) + W_- I_{1^-}^{2-\alpha} Q_m^{\mu,\nu}(x) = \tilde{A}_m P_m^{\nu,\mu}(x). \tag{5.13}$$

Now divide both sides of (5.13) by $W_+ + W_-$ and let

$$p = \frac{W_+}{W_+ + W_-} = \frac{\sin(\pi\gamma) + \cos(\pi\gamma)\tan((\alpha-1)\pi/2)}{2\sin(\pi\gamma)} \tag{5.14a}$$

$$q = \frac{W_-}{W_+ + W_-} = \frac{\sin(\pi\gamma) - \cos(\pi\gamma)\tan((\alpha-1)\pi/2)}{2\sin(\pi\gamma)} \tag{5.14b}$$

which is valid for $0 < \gamma < 1$. Solve (5.10a) for $\gamma = (\alpha-1)/2 - \mu$ and subtract (5.14b) from (5.14a), yielding (5.9b). Add (5.10a) and (5.10b), yielding (5.9a). Finally, divide (5.12) by $W_+ + W_-$, yielding (5.9c). □

Remark 5.4. Ervin et al. [21, Lemma 4.3] use the Gauss hypergeometric function ${}_2F_1(a, b; c; z)$ to reach a similar result in the special case of $m = 0$ on the interval [0,1].

Armed with Lemma 5.3, we can now compute the two-sided Riemann–Liouville derivative of the family of functions defined by $Q_m^{\mu,\nu}(x)$.

Theorem 5.5. *Let $\mathcal{D}_{RL}^{\alpha} = p\mathbb{D}_{-1^+}^{\alpha} + q\mathbb{D}_{1^-}^{\alpha}$ be the two-sided Riemann–Liouville derivative on $[-1, 1]$, with $1 < \alpha < 2$, $p + q = 1$, and let $m \geq 0$ be an integer. Then*

$$\mathcal{D}_{RL}^{\alpha} Q_m^{\mu,\nu}(x) = C_m \frac{\partial^2}{\partial x^2} P_m^{\nu,\mu}(x), \tag{5.15}$$

where $Q_m^{\mu,\nu}(x)$ is given by (5.5) and μ, ν, and C_m satisfy (5.9).

Proof. Apply the second derivative operator to (5.8). By (2.2), the theorem follows. □

Corollary 5.6. *The kernel of the two-sided Riemann–Liouville derivative on $[-1, 1]$ is given by $\ker(\mathcal{D}_{RL}^{\alpha}) = c_0 Q_0^{\mu,\nu}(x) + c_1 x Q_0^{\mu,\nu}(x)$, where $Q_0^{\mu,\nu}(x) = (1-x)^{\mu}(1+x)^{\nu}$.*

Proof. Let $m = 0$ in Theorem 5.5. The right-hand side of (5.15) vanishes since $P_0^{\nu,\mu}(x)$ is a constant. Likewise, let $m = 1$ in the same theorem. Since $P_1^{\nu,\mu}(x)$ is linear with respect to x, the right hand side of (5.15) also vanishes. □

Theorem 5.7. *The kernel of the two-sided Riemann–Liouville derivative on the interval $[-1, 1]$ is given by*

$$\ker(\mathcal{D}_{RL}^{\alpha}) = c_0(1-x)^{\mu}(1+x)^{\nu} + c_1 x(1-x)^{\mu}(1+x)^{\nu} \tag{5.16}$$

with parameters μ and ν satisfy (5.9a) and (5.9b). In particular, the steady state solution $u_\infty(x)$ subject to reflecting BCs (2.11) with $L = -1$ and $R = 1$ is

$$u_\infty(x) = \frac{M_0(1-x)^{\mu}(1+x)^{\nu}}{B(\mu+1, \nu+1)2^{1+\mu+\nu}} \tag{5.17}$$

where $B(\mu+1, \nu+1)$ is the beta function [22, Equation 2.5] and $M_0 = \int_{-1}^{1} u_0(x)\, dx$.

Proof. The kernel (5.16) follows immediately from Corollary 5.6. To demonstrate (5.17), the Riemann–Liouville flux $F_{RL}(x,t) = -p\partial/\partial x I_{-1^+}^{2-\alpha} u_\infty(x) + q\partial/\partial x I_{1^-}^{2-\alpha} u_\infty(x) = 0$, which is satisfied by $c_0 Q_0^{\mu,\nu}(x)$. Letting $M_0 = \int_{-1}^{1} u_0(x)\, dx$, we have

$$\begin{aligned}
M_0 &= \int_{-1}^{1} c_0(1-x)^{\mu}(1+x)^{\nu}\, dx \\
&= 2^{1+\mu+\nu} c_0 \int_{0}^{1} y^{\nu}(1-y)^{\mu}\, dy \\
&= 2^{1+\mu+\nu} c_0 B\left(\mu+1, \nu+1\right),
\end{aligned}$$

yielding the constant c_0. □

Remark 5.8. In the one-sided case ($p = 1$ and $q = 0$), (5.9a) and (5.9b) yield $\mu = 0$ and $\nu = \alpha - 2$. Evaluating the kernel (5.16) with these parameters yields

$$\begin{aligned}
\ker(\mathcal{D}_{RL}^{\alpha}) &= c_0(1+x)^{\alpha-2} + c_1 x(1+x)^{\alpha-2} \\
&= (c_0 - c_1)(x+1)^{\alpha-2} + c_1(x+1)^{\alpha-1},
\end{aligned}$$

which agrees with the known one-sided solution (5.1). Likewise, if $p = 0$ and $q = 1$, then (5.9a) and (5.9b) yield $\mu = \alpha - 2$ and $\nu = 0$, and (5.16) evaluates to $\ker(\mathcal{D}^{\alpha}_{RL}) = (c_0 + c_1)(1-x)^{\alpha-2} - c_1(1-x)^{\alpha-1}$.

Remark 5.9. In the symmetric case ($p = q = 1/2$), $\mu = \nu = \alpha/2 - 1$, yielding the kernel

$$\ker(\mathcal{D}^{\alpha}_{RL}) = c_0(1-x^2)^{\alpha/2-1} + c_1 x(1-x^2)^{\alpha/2-1},$$

which, in general, is singular at both $x = -1$ and $x = 1$. Setting $c_1 = c_0$, yields $\ker(\mathcal{D}^{\alpha}_{RL}) = c_0(1+x)^{\alpha/2}(1-x)^{\alpha/2-1}$, which is regular at $x = -1$ and singular at $x = 1$. Setting $c_1 = -c_0$ yields $\ker(\mathcal{D}^{\alpha}_{RL}) = c_0(1+x)^{\alpha/2-1}(1-x)^{\alpha/2}$, which is singular at $x = -1$ and regular at $x = 1$. The steady-state solution (5.17) with reflecting BCs with $B(\alpha/2, \alpha/2) = (\Gamma(\alpha/2))^2/\Gamma(\alpha)$ is

$$u_{\infty}(x) = M_0 \frac{\Gamma(\alpha)}{2^{\alpha-1}(\Gamma(\alpha/2))^2}(1-x^2)^{\alpha/2-1}, \tag{5.18}$$

which is symmetric about $x = 0$. If $\alpha = 1$, then (5.18) is proportional to the arc sine density [22, Equation 4.4] on the interval $[-1, 1]$.

5.2. Caputo flux

As with Riemann–Liouville flux, the kernel of the one-sided ($p = 1$) Patie–Simon derivative was computed in Baeumer et al. [6],

$$\ker\left(\mathbf{D}^{\alpha}_{-1^+}\right) = c_0 + c_1(x+1)^{\alpha-1}, \tag{5.19}$$

where c_0 and c_1 are arbitrary constants. Unlike (5.1), (5.19) is regular at both end-points. The only steady solution with total mass of one that satisfies reflecting BCs (2.12b) is $u_{\infty}(x) = 1/2$. In this section, we compute the kernel of the two-sided Patie–Simon derivative $\ker\left(\mathcal{D}^{\alpha}_{PS}\right)$

$$p\mathbf{D}^{\alpha}_{-1^+}u_{\infty}(x) + q\mathbf{D}^{\alpha}_{1^+}u_{\infty}(x) = 0. \tag{5.20}$$

This task requires another technical lemma.

Lemma 5.10. *Let μ and ν satisfy (5.10). Then*

$$\int_{-1}^{x}(1-y)^{\mu}(1+y)^{\nu}\,dy = \frac{2^{\mu}}{1+\nu}(1+x)^{1+\nu}{}_2F_1(-\mu, 1+\nu; 2+\nu; (1+x)/2), \tag{5.21}$$

where the Gauss hypergeometric function ${}_2F_1(a, b; c; w)$ has an integral representation given by [23, Section 1.6]

$$ {}_2F_1(a, b; c; w) = \frac{\Gamma(c)}{\Gamma(b)\Gamma(c-b)}\int_0^1 z^{b-1}(1-z)^{c-b-1}(1-zw)^{-a}\,dz \tag{5.22}$$

with $0 < b < c$.

Proof. Let $z = (y+1)/(x+1)$ in (5.21), yielding

$$\int_{-1}^{x}(1-y)^{\mu}(1+y)^{\nu}\,dy = (x+1)^{\nu+1}2^{\mu}\int_0^1 z^{\nu}(1-zw)^{\mu}\,dz,$$

where $w = (1+x)/2$. Compare to (5.22) with $a = -\mu$, $b = 1+\nu$ and $c = 2+\nu$ and note that $\Gamma(1+\nu)\Gamma(1)/\Gamma(2+\nu) = 1/(1+\nu)$, yielding (5.21). $\square$

Theorem 5.11. *The kernel of the two-sided Patie–Simon derivative on the interval $[-1, 1]$ is given by*

$$\ker\left(\mathcal{D}^{\alpha}_{PS}\right) = c_0 + c_1(1+x)^{1+\nu}{}_2F_1(-\mu, 1+\nu; 2+\nu; (1+x)/2) \tag{5.23}$$

with parameters μ and ν satisfy (5.9a) and (5.9b). In particular, the steady state solution $u_{\infty}(x)$ subject to reflecting BCs (2.11b) with $L = -1$ and $R = 1$ is $u_{\infty}(x) = M_0/2$, where M_0 is the total mass.

Proof. Let $\mathcal{D}^{\alpha}_{PS} = p\mathbf{D}^{\alpha}_{-1+} + q\mathbf{D}^{\alpha}_{1-}$ be the two-sided Patie–Simon derivative and define

$$u(x) = c_0 + c_1 \int_{-1}^{x} Q_0^{\mu,\nu}(y)\,dy.$$

By (2.6),

$$\begin{aligned}\mathcal{D}^{\alpha}_{PS} u_\infty(x) &= \left(p\mathbf{D}^{\alpha}_{-1+} + q\mathbf{D}^{\alpha}_{1-}\right) u(x)\\ &= \frac{\partial}{\partial x}\left(pI^{2-\alpha}_{-1+} + qI^{2-\alpha}_{1-}\right)\frac{\partial}{\partial x} u(x)\\ &= \frac{\partial}{\partial x}\left(pI^{2-\alpha}_{-1+} + qI^{2-\alpha}_{1-}\right) c_1 Q_0^{\mu,\nu}(x).\end{aligned}$$

By (5.8), we have

$$\mathcal{D}^{\alpha}_{PS} u_\infty(x) = c_1 C_0 \frac{\partial}{\partial x} P_0^{\nu,\mu}(x) = 0.$$

Then invoke (5.21), thus proving (5.23). Of the two terms in (5.23), only $u_\infty(x) = c_0$ satisfies the reflecting BCs (2.11b). Then $\int_{-1}^{1} c_0\,dx = M_0$, yielding $c_0 = M_0/2$. □

Remark 5.12. Ervin et al. [21, Corollary 4.1] also computed the kernel of $\mathcal{D}^{\alpha}_{PS}$ on [0, 1], yielding similar expressions involving the Gauss hypergeometric function.

Remark 5.13. In the one-sided case ($p = 1$ and $q = 0$), $\mu = 0$ and $\nu = \alpha - 2$. Evaluating (5.23) yields

$$\begin{aligned}\ker\left(\mathcal{D}^{\alpha}_{PS}\right) &= c_0 + c_1(1+x)^{\alpha-1}{}_2F_1(0, \alpha-1; \alpha; (1+x)/2)\\ &= c_0 + c_1(x+1)^{\alpha-1}\end{aligned}$$

which agrees with (5.19).

6. Numerical experiments

6.1. One-sided fractional derivative

In our first experiment, we use the method of manufactured solutions (MOMS) to test the convergence of the one-sided fractional diffusion equations using both the Riemann–Liouville derivative and the Patie–Simon given by (2.1) and (2.5), respectively. We assume reflecting boundary conditions at both $x = -1$ and $x = 1$. To construct an initial condition, we first identify the domains of the positive Riemann–Liouville derivative and positive Patie–Simon derivative that satisfy reflecting BCs on the interval $[-1, 1]$ [6, Table 1, Rows 6 and 4]:

$$\mathrm{Dom}\left(\mathbb{D}^{\alpha}_{-1+}, NN\right) = \left\{ f \in X : f = I^{\alpha}_{-1+}g - \frac{I^{1}_{-1+}g(1)}{p_1^+(1)} p_\alpha^+(x) + c p^+_{\alpha-2}(x),\ g \in X \right\} \tag{6.1a}$$

$$\mathrm{Dom}\left(\partial^{\alpha}_{-1+}, NN\right) = \left\{ f \in X : f = I^{\alpha}_{-1+}g - \frac{I^{1}_{-1+}g(1)}{p_1^+(1)} p_\alpha^+(x) + c p^+_{0}(x),\ g \in X \right\} \tag{6.1b}$$

where NN denotes the Neumann BCs in (2.12a) and (2.12b), $p_\alpha^+(x) = (1+x)^\alpha/\Gamma(\alpha+1)$, $c \in \mathbb{R}$, and X is some suitable space of functions (e.g., $X = L_1[-1, 1]$). By choosing $g(x) = -(1+x)^\beta$ where $\beta > 0$ in (6.1a) and (6.1b) and $c = 0$, we construct an initial condition

$$u_0(x) = \frac{2^\beta}{1+\beta} p_\alpha^+(x) - \Gamma(1+\beta) p^+_{\alpha+\beta}(x). \tag{6.2}$$

Since $\mathrm{Dom}\left(\mathbb{D}^{\alpha}_{-1+}, NN\right) = \mathrm{Dom}\left(\partial^{\alpha}_{-1+}, NN\right)$ for $c = 0$, (6.2) is a valid initial condition for both (2.1) and (2.5). The manufactured source term $s(x, t)$ is given by

$$s(x,t) = -e^{-t}\left(u_0(x) + \frac{2^\beta}{1+\beta} - \Gamma(\beta+1) p_\beta^+(x)\right), \tag{6.3}$$

yielding an exact analytical solution

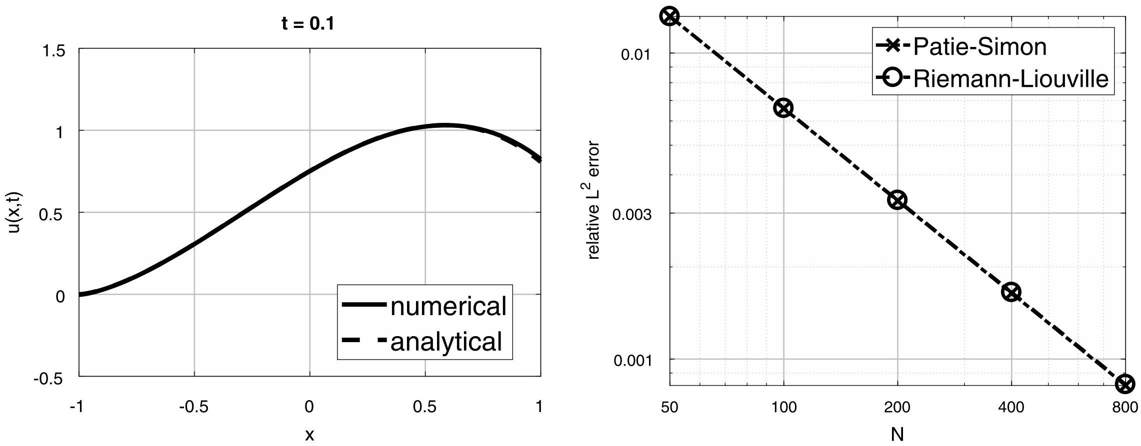

(a) Solution using $n = 100$ grid points

(b) convergence study

Fig. 1. Panel (a) compares the exact solution (6.4) of (2.1) using the Riemann–Liouville derivative with the numerical solution using $n = 100$ grid points and $\alpha = 1.5$. The numerical solution of (2.5) using the Patie–Simon derivative with the same parameters is very similar.

$$u(x,t) = u_0(x)e^{-t}. \tag{6.4}$$

Equations (2.1) and (2.5) are discretized using the explicit Euler scheme (3.4) and simulated with a uniform grid of n points, where $n =$ 50, 100, 200, 400, and 800 with $\alpha = 1.5$ and $\beta = 2$. A time-step satisfying $\Delta t \le h^\alpha/\alpha$ is chosen and the relative L^2 error between the exact and numerical solutions is computed after 2000 timesteps. Fig. 1a compares the exact solution (6.4) with the numerical solution using $n = 100$ grid points, while Fig. 1b displays the relative L^2 error as a function n for both models. In panel a, there is good agreement between the numerical and analytical solution, although there is some disagreement near the right boundary. The numerical solution of (2.5) using the Patie–Simon derivative with the same parameters behaves in the same manner. As the grid is refined (n increases), the numerical solutions using either the Riemann–Liouville and Patie–Simon derivatives converge to the exact solution, as shown in panel b. The numerical convergence rate for both the Riemann–Liouville and Patie–Simon diffusion equations, which is given by the negative of the slope of Fig. 1b, is approximately one, which agrees with the truncation error of the shifted Grünwald estimate. The measured numerical convergence rate of the Patie–Simon diffusion equation suggests that the truncation error associated with the iteration matrix (3.9) is $\mathcal{O}(h)$ even though this scheme contains an approximation of $g_{j+1}^{\alpha-1}$ [5, Equation (6.8)].

6.2. Two-sided fractional derivative

In the following numerical experiments, we used $\Delta x = 1/500$ with $n = 1000$ grid-points and the implicit scheme (3.7) with a time-step of $\Delta t = 0.0025$. We have verified these results by reproducing these results using the explicit Euler scheme (3.5) with a time-step of $\Delta t = 0.0002$, which satisfies the stability limit in Proposition 4.3. A tent function initial condition

$$u_0(x) = \begin{cases} 5 - 25|x| & \text{for } |x| < 0.2, \\ 0 & \text{otherwise,} \end{cases} \tag{6.5}$$

with mass $M_0 = 1$.

Fig. 2 shows numerical solutions for the fractional diffusion equation with Riemann–Liouville flux using $\alpha = 1.5$ and reflecting BCs at both end-points. The weight p varies from a) $p = 1$, b) $p = 0.75$, c) $p = 0.5$, and d) $p = 0.25$, and solutions are shown at $t = 0$ (solid), $t = 0.05$ (dotted), $t = 0.1$ (dash-dotted) and $t = 2$ (dashed), while the steady-state solution (5.17) is shown with circles. In the one-sided case shown in panel a, the numerical solution is singular at $x = -1$ but regular at $x = 1$. In contrast, the numerical solutions in panels b), c), and d) are singular at both $x = -1$ and $x = 1$.

Fig. 3 displays solutions of the fractional diffusion equation (Caputo flux) with $\alpha = 1.5$ and $p = 0.25$ using a) absorbing BCs, b) absorbing-reflecting BCs, c), reflecting-absorbing BCs, and d) reflecting BCs at $t = 0$ (solid), $t = 0.05$ (dotted), $t = 0.1$ (dash-dotted) and $t = 2$ (dashed). In panel d), the steady-state solution $u_\infty(x) = 1/2$ is shown (circles). In panels a, b, and c, the numerical solutions tend toward a steady state of zero. In panel d, which uses reflecting BCs, the numerical solutions tend toward a steady state of $u_\infty(x) = 1/2$. Unlike solutions using the Riemann–Liouville flux, the solutions using Caputo flux are regular at both end-points for all BC choices. Numerical solutions using the Riemann–Liouville flux and absorbing BCs are identical to Fig. 3a for the same choice of α and p since the two derivatives are equal in this case by (2.8).

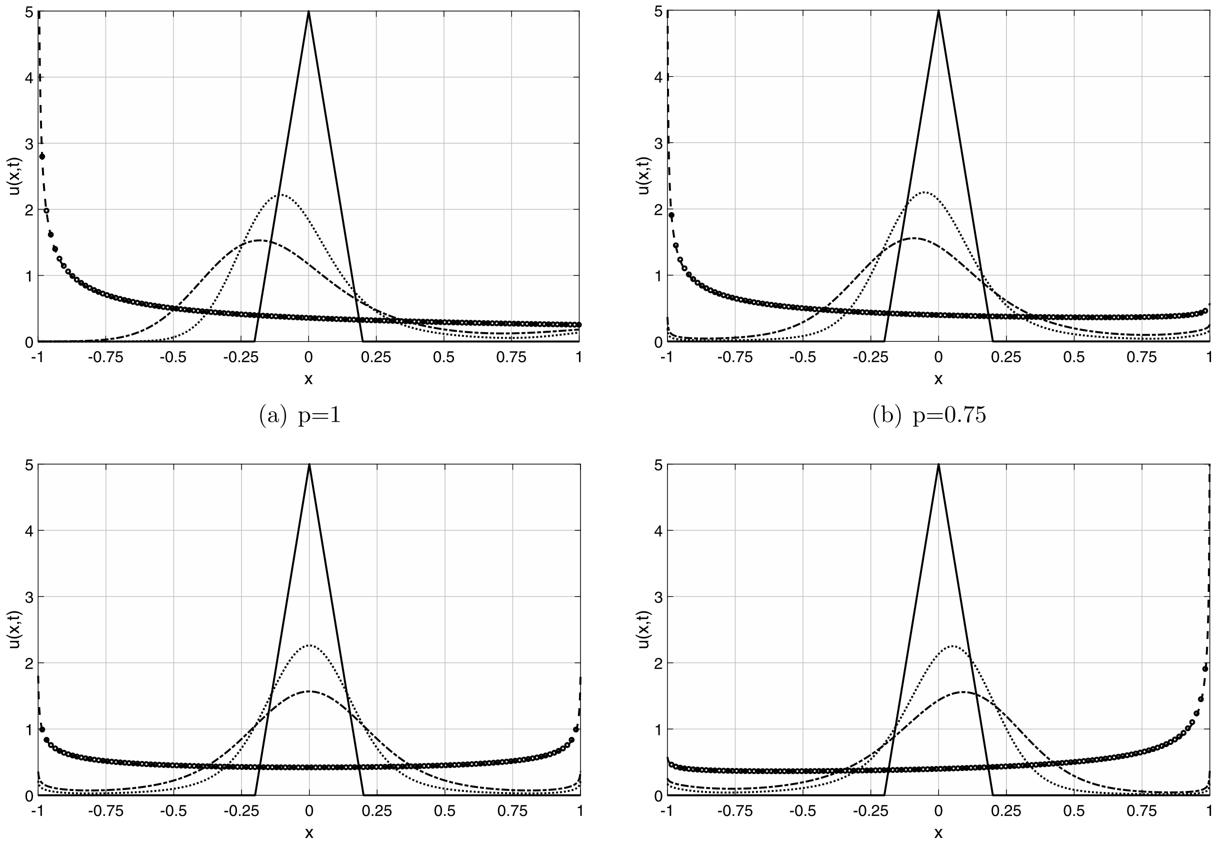

(a) p=1 (b) p=0.75

(c) p=0.5 (d) p=0.25

Fig. 2. Solutions of the fractional diffusion equation (Riemann–Liouville flux) with $\alpha = 1.5$, $C = 1$, and reflecting BCs at both end-points. The parameter p varies from (a) $p = 1$, (b) $p = 0.75$, (c) $p = 0.5$, and (d) $p = 0.25$. $t = 0$ (solid), $t = 0.05$ (dotted), $t = 0.1$ (dash-dotted) and $t = 2$ (dashed), and the steady-state solution (circles).

7. Discussion

For diffusion with Riemann–Liouville flux shown in Fig. 2, the presence of the reflecting boundary has a profound impact on the solution as time evolves: there is a build-up of mass near the wall, yielding a steady state solution that exhibits a singularity at each boundary. From a particle point of view, there is a build-up of particles at both boundaries for $0 < p < 1$. In contrast, the diffusion equation with Caputo flux equipped with reflecting BCs in Fig. 3d has a constant steady state solution for all $0 \le p \le 1$, agreeing with both the classical diffusion case ($\alpha = 2$) and the one-sided fractional diffusion equation with Caputo flux [5]. Consideration of the steady state behavior can be a useful guide in model selection.

Remark 7.1. The explicit and implicit Euler schemes given in Section 3 are low-order with an error term $\mathcal{O}(h)$. High-order, stable schemes for fractional BVPs with absorbing BCs were proposed in [4,10,46]. It would be interesting to augment these high-order schemes with reflecting boundary conditions, yielding efficient, high-order methods for problems with a range of boundary conditions. Development of spectral methods for reflecting BCs using orthogonal polynomials (i.e., poly-fractonomials), which are currently limited to Dirichlet (absorbing) BCs [29,30,51,42], would also be interesting. As noted in [30], the two-sided polyfractonomials $Q_m^{\mu,\nu}(x)$ capture the singular behavior of the Riemann–Liouville operator near the boundary.

Remark 7.2. Section 4 has shown stability for the explicit and implicit Euler schemes. Since these methods are also consistent, these schemes are convergent by the Lax equivalence theorem [41]. Several results establishing well-posedness in the *weak sense* of steady-state space-fractional diffusion equations subject to reflecting boundary conditions have recently appeared. Wang et al. [48] showed weak well-posedness for the one-sided Riemann–Liouville steady-state diffusion equation with a positive $\alpha - 1$ derivative at $x = L$ and a negative $\alpha - 1$ derivative at $x = R$. Ma [28] established weak well-posedness of the two-sided steady-state Patie–Simon diffusion equation (two-sided Caputo flux) with a fractional Robin BC that employs the $\alpha - 1$ Caputo derivative using the Lax–Milgram theorem. This fractional Robin BC reduces to (2.11b)

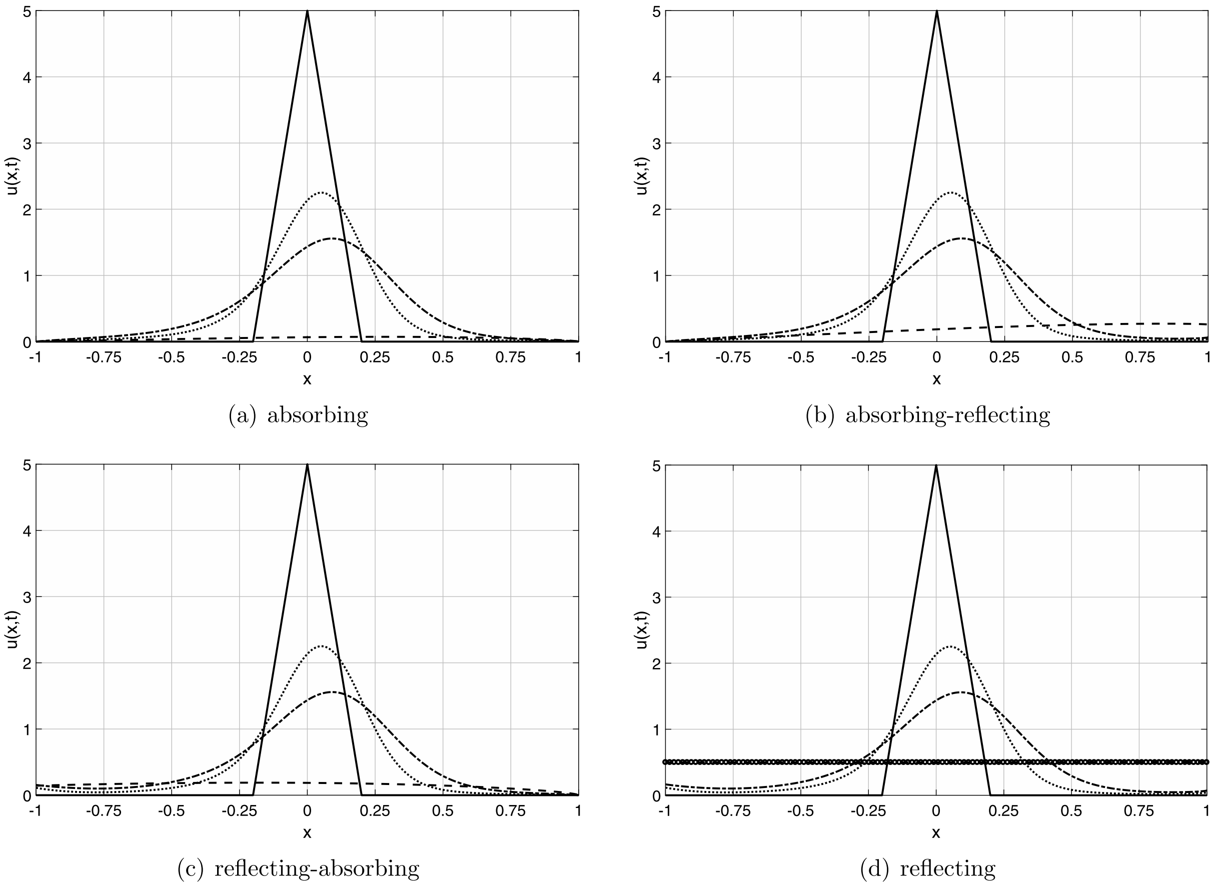

Fig. 3. Solutions of the fractional diffusion equation (Caputo flux) with $\alpha = 1.5$, $C = 1$, and $p = 0.25$ using a) absorbing BCs, b) absorbing-reflecting BCs, c), reflecting-absorbing BCs, and d) reflecting BCs at $t = 0$ (solid), $t = 0.05$ (dotted), $t = 0.1$ (dash-dotted) and $t = 2$ (dashed). In panel d), the steady-state solution $u_\infty(x) = 1/2$ is shown (circles).

for an appropriate choice of coefficients. Wang et al. [49] extended these results to the steady-state Riemann–Liouville diffusion equation using a similar approach. Deng et al. [18] also established weak well-posedness for the symmetric time-dependent diffusion equation using a different definition of the fractional Laplacian where the integration extends over all of $\mathbb{R}^n$.

Unlike the one-sided case [6], well-posedness in the *strong sense* for Cauchy problems using the two-sided time-dependent diffusion equations subject to reflecting BCs remains an open problem. To prove well-posedness, the approach of Baeumer et al. [6] may be fruitful, which requires identification of the domains of the two-sided fractional derivatives $\mathrm{Dom}(\mathcal{D}^\alpha_{RL})$ and $\mathrm{Dom}(\mathcal{D}^\alpha_{PS})$ for each pair of boundary conditions. The kernels computed in Section 5 may be used to construct these domains. It may be possible to use the kernels computed in Section 5 to construct these domains and then show that $\mathcal{D}^\alpha_{RL}$ and $\mathcal{D}^\alpha_{PS}$ equipped with reflecting BCs generate strongly continuous contraction semi-groups on an appropriate space of functions (e.g., $L^1[L, R]$ or $C[L, R]$).

8. Conclusions

This paper has established appropriate absorbing (Dirichlet) and reflecting (Neumann) boundary conditions for two versions of the two-sided, space-fractional diffusion equation, thus extending the scheme developed for the one-sided case in Baeumer et al. [5]. By expressing the fractional diffusion equation in conservation form, two flux functions were identified: the Riemann–Liouville flux and the Caputo flux. A conditionally stable explicit Euler scheme and an unconditionally stable implicit Euler scheme were proposed using the shifted Grünwald estimate from Meerschaert and Tadjeran [33], and stability was demonstrated using the Gerschgorin circle theorem. Steady state solutions subject to reflecting BCs using Riemann–Liouville flux are singular at one or more of the end-points, while steady-state solutions subject to reflecting BCs using Caputo flux are constant functions. Numerical experiments illustrated the convergence of the explicit and implicit methods. Finally, the influence of the reflecting boundary on the steady-state behavior subject to both the Riemann–Liouville and Caputo fluxes was discussed.

Acknowledgements

Kelly was partially supported by ARO MURI grant W911NF-15-1-0562 and USA National Science Foundation grant EAR-1344280. Meerschaert was partially supported by ARO MURI grant W911NF-15-1-0562 and USA National Science Foundation grant DMS-1462156 and EAR-1344280. We thank Mohsen Zayernouri (Dept. of Computational Science and Engineering, Michigan State University) for insightful discussion and for bringing reference [2] to our attention.

References

[1] M. Abramowitz, I.A. Stegun, Handbook of Mathematical Functions: With Formulas, Graphs, and Mathematical Tables, Dover, New York, 1972.
[2] R. Askey, J. Fitch, Integral representations for Jacobi polynomials and some applications, J. Math. Anal. Appl. 26 (2) (1969) 411–437.
[3] K.E. Atkinson, An Introduction to Numerical Analysis, John Wiley & Sons, New York, 1989.
[4] B. Baeumer, M. Kovács, H. Sankaranarayanan, Higher order Grünwald approximations of fractional derivatives and fractional powers of operators, Trans. Am. Math. Soc. 367 (2) (2015) 813–834.
[5] B. Baeumer, M. Kovács, M.M. Meerschaert, H. Sankaranarayanan, Boundary conditions for fractional diffusion, J. Comput. Appl. Math. 336 (2018) 408–424.
[6] B. Baeumer, M. Kovács, H. Sankaranarayanan, Fractional partial differential equations with boundary conditions, J. Differ. Equ. 264 (2018) 1377–1410.
[7] D.A. Benson, S.W. Wheatcraft, M.M. Meerschaert, Application of a fractional advection–dispersion equation, Water Resour. Res. 36 (2000) 1403–1412.
[8] D.A. Benson, R. Schumer, M.M. Meerschaert, S.W. Wheatcraft, Fractional dispersion, Lévy motion, and the MADE tracer tests, Transp. Porous Media 42 (2001) 211–240.
[9] N. Burch, R.B. Lehoucq, Continuous-time random walks on bounded domains, Phys. Rev. E 83 (1) (2011) 012105.
[10] M. Chen, W. Deng, Fourth order accurate scheme for the space fractional diffusion equations, SIAM J. Numer. Anal. 52 (3) (2014) 1418–1438.
[11] W. Chen, A speculative study of 2/3-order fractional Laplacian modeling of turbulence: some thoughts and conjectures, Chaos 16 (2006) 023126.
[12] N. Cusimano, K. Burrage, I. Turner, D. Kay, On reflecting boundary conditions for space-fractional equations on a finite interval: proof of the matrix transfer technique, Appl. Math. Model. 42 (2017) 554–565.
[13] O. Defterli, M. D'Elia, Q. Du, M. Gunzburger, R. Lehoucq, M.M. Meerschaert, Fractional diffusion on bounded domains, Fract. Calc. Appl. Anal. 18 (2) (2015) 342–360.
[14] D. del-Castillo-Negrete, B.A. Carreras, V.E. Lynch, Fractional diffusion in plasma turbulence, Phys. Plasmas 11 (8) (2004) 3854.
[15] D. del Castillo-Negrete, Fractional diffusion models of nonlocal transport, Phys. Plasmas 13 (8) (2006) 082308.
[16] M. D'Elia, M. Gunzburger, The fractional Laplacian operator on bounded domains as a special case of the nonlocal diffusion operator, Comput. Math. Appl. 66 (7) (2013) 1245–1260.
[17] S. Duo, H. Wang, Y. Zhang, A comparative study on nonlocal diffusion operators related to the fractional Laplacian, Preprint, https://arxiv.org/pdf/1711.06916.pdf, 2017.
[18] W. Deng, B. Li, W. Tian, P. Zhang, Boundary problems for the fractional and tempered fractional operators, SIAM J. Multiscale Model. Simul. 16 (1) (2018) 125–149.
[19] S. Dipierro, X. Ros-Oton, E. Valdinoci, Nonlocal problems with Neumann boundary conditions, Rev. Mat. Iberoam. 33 (2017) 377–416.
[20] B.P. Epps, B. Cushman-Roisin, Turbulence modeling via the fractional Laplacian, Preprint, arXiv:1803.05286 [.org/abs], 2018.
[21] V. Ervin, N. Heuer, J. Roop, Regularity of the solution to 1-d fractional order diffusion equations, Math. Comput. 87 (2018) 2273–2294.
[22] W. Feller, An Introduction to Probability Theory and its Applications, vol. 2, John Wiley & Sons, New York, 2008.
[23] A.A. Kilbas, H.M. Srivastava, J.J. Trujillo, Theory and Applications of Fractional Differential Equations, Elsevier Science Limited, Amsterdam, 2006.
[24] M. Gunzburger, N. Jian, F. Xu, Analysis and approximation of a fractional Laplacian-based closure model for turbulent flows and its connection to Richardson pair dispersion, Comput. Math. Appl. 75 (6) (2018) 1973–2001.
[25] S. Kim, M.L. Kavvas, Generalized Fick's law and fractional ADE for pollution transport in a river: detailed derivation, J. Hydrol. Eng. 11 (1) (2006) 80–83.
[26] N. Krepysheva, L. Di Pietro, M.-C. Néel, Fractional diffusion and reflective boundary condition, Phys. A, Stat. Mech. Appl. 368 (2) (2006) 355–361.
[27] A. Lischke, G. Pang, M. Gulian, F. Song, C. Glusa, X. Zheng, Z. Mao, W. Cai, M.M. Meerschaert, M. Ainsworth, G.E. Karniadakis, What is the fractional Laplacian? Preprint, https://arxiv.org/pdf/1801.09767.pdf.
[28] J. Ma, A new finite element analysis for inhomogeneous boundary-value problems of space fractional differential equations, J. Sci. Comput. 70 (1) (2017) 342–354.
[29] Z. Mao, S. Chen, J. Shen, Efficient and accurate spectral method using generalized Jacobi functions for solving Riesz fractional differential equations, Appl. Numer. Math. 106 (2016) 165–181.
[30] Z. Mao, G.E. Karniadakis, A spectral method (of exponential convergence) for singular solutions of the diffusion equation with general two-sided fractional derivative, SIAM J. Numer. Anal. 56 (1) (2018) 24–49.
[31] M.M. Meerschaert, D.A. Benson, B. Baeumer, Operator Lévy motion and multiscaling anomalous diffusion, Phys. Rev. E 63 (2001) 021112.
[32] M.M. Meerschaert, A. Sikorskii, Stochastic Models for Fractional Calculus, vol. 43, Walter de Gruyter, Berlin, 2012.
[33] M.M. Meerschaert, C. Tadjeran, Finite difference approximations for fractional advection–dispersion flow equations, J. Comput. Appl. Math. 172 (1) (2004) 65–77.
[34] M.M. Meerschaert, C. Tadjeran, Finite difference approximations for two-sided space-fractional partial differential equations, Appl. Numer. Math. 56 (1) (2006) 80–90.
[35] S. Mittnik, S.T. Rachev, Option pricing for stable and infinitely divisible asset returns, Math. Comput. Model. 29 (1999) 93–104.
[36] P. Paradisi, R. Cesari, F. Mainardi, F. Tampieri, The fractional Fick's law for non-local transport processes, Phys. A, Stat. Mech. Appl. 293 (1) (2001) 130–142.
[37] P. Patie, T. Simon, Intertwining certain fractional derivatives, Potential Anal. 36 (4) (2012) 569–587.
[38] I. Podlubny, Fractional Differential Equations, Academic Press, San Diego, 1999.
[39] I. Podlubny, A. Chechkin, T. Skovranek, Y. Chen, B.M.V. Jara, Matrix approach to discrete fractional calculus, II: partial fractional differential equations, J. Comput. Phys. 228 (8) (2009) 3137–3153.
[40] G.Y. Popov, Some properties of classical polynomials and their application to contact problems, Prikl. Math. Mekh. (Russian) 27 (1963) 821–832.
[41] R.D. Richtmyer, Difference Methods for Initial-Value Problems, Interscience Publishers, Inc., New York, 1957.
[42] M. Samiee, M. Zayernouri, M.M. Meerschaert, A unified spectral method for FPDEs with two-sided derivatives; part I: a fast solver, J. Comput. Phys. (2018), in press.
[43] S.G. Samko, A.A. Kilbas, O.I. Marichev, Fractional Integrals and Derivatives: Theory and Applications, Gordon and Breach, London, 1993.
[44] R. Schumer, D.A. Benson, M.M. Meerschaert, S.W. Wheatcraft, Eulerian derivation of the fractional advection–dispersion equation, J. Contam. Hydrol. 48 (1) (2001) 69–88.

[45] S.A. Silling, Reformulation of elasticity theory for discontinuities and long-range forces, J. Mech. Phys. Solids 48 (1) (2000) 175–209.
[46] W. Tian, H. Zhou, W. Deng, A class of second order difference approximations for solving space fractional diffusion equations, Math. Comput. 84 (294) (2015) 1703–1727.
[47] B.E. Treeby, B. Cox, Modeling power law absorption and dispersion for acoustic propagation using the fractional Laplacian, J. Acoust. Soc. Am. 127 (5) (2010) 2741–2748.
[48] H. Wang, D. Yang, Wellposedness of Neumann boundary-value problems of space-fractional differential equations, Fract. Calc. Appl. Anal. 20 (6) (2017) 1356–1381.
[49] N. Wang, Z. Mao, C. Huang, G.E. Karniadakis, A spectral penalty method for two-sided fractional differential equations with general boundary conditions, preprint, https://arxiv.org/abs/1807.04684, 2018.
[50] G.M. Viswanathan, V. Afanasyev, S.V. Buldyrev, E.J. Murphy, P.A. Prince, H.E. Stanley, Lévy flight search patterns of wandering albatrosses, Nature 381 (1996) 413–415.
[51] M. Zayernouri, G.E. Karniadakis, Fractional spectral collocation method, SIAM J. Sci. Comput. 36 (1) (2014) A40–A62.
[52] X. Zhang, M. Lv, J.W. Crawford, I.M. Young, The impact of boundary on the fractional advection–dispersion equation for solute transport in soil: defining the fractional dispersive flux with the Caputo derivatives, Adv. Water Resour. 30 (5) (2007) 1205–1217.